Materials Research Express

PAPER

Physical properties of cost effectively synthesized ZnO nanowires post annealed under various thermal and atmosphere treatments for UV photodetectors

To cite this article: R Bahramian *et al* 2019 *Mater. Res. Express* **6** 045906

Materials Research Express

RECEIVED
6 August 2018

REVISED
5 December 2018

ACCEPTED FOR PUBLICATION
2 January 2019

PUBLISHED
18 January 2019

PAPER

Physical properties of cost effectively synthesized ZnO nanowires post annealed under various thermal and atmosphere treatments for UV photodetectors

R Bahramian[1,2], A Moshaii[1] and H Eshghi[2]

[1] Department of physics, Tarbiat Modares University, Tehran, PO Box 14115-175, Iran
[2] Department of physics, Shahrood University of Technology, Shahrood, PO Box 36199-95161, Iran

E-mail: bahramian_reyhaneh@yahoo.com

Keywords: ZnO nanowires, chemical bath deposition, annealing effect, UV photodetector

Abstract

Vertically aligned Zinc Oxide nanowires (ZnO NWs) were grown on glass seeded substrates by the chemical bath deposition (CBD) method at a low temperature. Two parameters including temperature and atmosphere were varied while time and heating rate were kept constant. The field emission scanning electron microscopy images show that the ZnO NWs with a hexagonal cross section are grown perpendicular to the seeded glass substrates. The x-ray diffraction results reveal that all the ZnO NW arrays grow preferentially oriented along the c-axis in the direction of (002) plane with a hexagonal wurtzite structure. Photoluminescence measurements of the grown ZnO NWs on all samples exhibit a high ultraviolet (UV) peak intensity compared to a broad visible peak, which can be accounted for the formation of the high crystal quality ZnO NWs. Results show that the UV light emission is greatly enhanced by annealing the as-grown ZnO NWs in O_2 ambient. Moreover, transient response measurement reveals that the detectors exhibit a fast photoresponse time of fewer than 5 s. In this annealing case, the quantum efficiency of UV detection reaches about 15%. Finally, a qualified metal-semiconductor-metal (MSM) ZnO photodetector was prepared from the annealed as-grown sample in the pure O_2 ambient.

1. Introduction

Over the past few years, zinc oxide (ZnO) has attracted a great attention because of its special properties. This oxide has a direct bandgap of 3.37 eV at room temperature and a large exciton binding energy of 60 meV with an n-type conductivity [1–4]. Other properties of ZnO are its high transparency, piezoelectricity, biocompatibility and capability to synthesize with different shapes [5–9] that allow various novel devices to be constructed. Due to these unique properties of ZnO, it is suitable candidate for various fields of applications such as blue-ultraviolet light emitters [10], photodetectors [11–13], memory devices [14], transparent electrodes, dye-sensitized solar cells [15, 16] and photocatalysis [17, 18].

Ultraviolet (UV) Photodetectors based on ZnO have attracted researchers in recent years due to their use in solar UV radiation detection, flame monitoring, chemical and biological sensors, and so on [19].

In UV photodetectors, the amount of surface exposed to direct incident light is important. By increasing the surface, the detector's sensitivity to UV light is increased. Nanostructured ZnO in the shape of the nanowire (NW) has the high surface-to-volume ratio in compared with thin film. Vertical NWs are more exposed to UV light compared to the horizontal ones because the NWs in a horizontal position prevent the incident light arriving at others. In horizontal mode, the high surface-to-volume ratio is not efficient. One of the most common configurations of UV photodetectors is the metal-semiconductor-metal (MSM) photodetectors owing to their simplicity in design and fabrication, large active area, fast response and low dark current [19].

Various techniques such as pulsed laser deposition [20], metal-organic chemical vapor deposition (MOCVD) [21], reactive evaporation, atomic layer deposition (ALD) [22, 23], chemical bath deposition (CBD)

[24–26], hydrothermal [5, 27–30], and even top-down approaches by etching [31] have been used to deposit ZnO thin films. Among these methods, CBD possesses many advantages including simplicity, large area to volume ratio, low-cost and low temperature [32, 33]. In addition, this method can be used to grow ZnO in the form of a nanowire, which is suitable for photodetector applications.

For producing uniform growth of a ZnO layer, seeding modification of the substrate is mandatory. In fact, the lattice mismatch and strain between the substrate and the zinc oxide crystal prevents proper growth of the ZnO layer. Therefore, the seed layer which is informed with spreading of ZnO nanoparticles over the substrate is necessary to eliminate the mismatch and strain. Also, the use of seed nanoparticles provides better alignment for the grown nanostructures [34]. The ZnO seed layer was prepared by RF magnetron sputtering at room temperature, where applying this method led to the synthesis of films with the highest quality and packing density [17, 35].

The high-range temperature used in this methods of fabrication of ZnO usually have restriction in using glass or plastic substratets, since they can only sustain temperatures up to 500 °C [36]. Therefore, the effects of annealing treatment at a lower temperature in different atmospheres need to be investigated for a variety of applications where the glass or plastic substrates are used. Accordingly, the optimum conditions in fabrication of ZnO NW arrays with low temperature CBD method, should be specified.

The effect of low-temperature annealing on the physical properties of ZnO thin films have been investigated in the literatures [37, 38]. However, the effect of heat treatment on defects, especially on UV-detection properties and the influence of various atmospheres were not carefully investigated.

In the present study, we report a comprehensive study on the structural, optical, and photoconductive properties of ZnO NW arrays grown on seeded glass substrates by CBD and its application in the UV MSM photodetectors. Then, the effects of the low range annealing temperature and various atmospheres on the ZnO NW arrays are studied. The results indicate that the annealing of NWs in various atmospheres at 400 °C provides very good crystalline structure for the NWs. However, annealing of the NWs in oxygen medium remarkably increases the UV detection properties of the NWs. We show that the optimized ZnO NWs by post-annealing in oxygen leads to fabricate inexpensive and commercial UV photodetector devices.

2. Materials and methods

2.1. Seeding procedure

All chemicals compounds were purchased from Merck and used as received. The glass substrates were initially cleaned with acetone in an ultrasonic bath, rinsed with deionized water, and then blown dry with the air flow. Then, a 100-nm ZnO seed layer was deposited by a radio frequency reactive magnetron sputtering [39] from a ZnO target, with the sputtering chamber pressure of 30 mTorr and a target-to-substrate separation of 7 cm. Sputtering was carried out at an incident power of 100 W for 30 min under the constant argon flow rate of 20 sccm (standard cubic centimeters per minute).

2.2. Growth of ZnO nanowires

ZnO NWs were grown on the glass substrate functionalized with the ZnO seed by a chemical bath deposition method [39, 40]. In brief, the nutrient solution was an aqueous solution of 16 mmol L^{-1} zinc nitrate hexahydrate ($Zn(NO_3)2{\cdot}6H_2O$, 98%) and 24 mmol L^{-1} hexamethylenetetramine (HMT: $C_6H_{12}N_4$, 99%). The reaction was kept at 90 °C for 3.5 h. For removing the samples from the solution, they were rinsed with deionized (DI) water and ethanol. Then, the samples were dried with air flow.

The influence of post-annealing was investigated in two states. The obtained ZnO NW arrays were annealed at 350, 400, and 450 °C in the air atmosphere to study the effect of annealing temperature. Then, the effect of annealing under various atmospheres was investigated by annealing the ZnO NW arrays at 400 °C in the air, pure oxygen, and pure argon atmospheres. The flow rate of oxygen and argon was 10 sccm. All samples were heated for one hour at a heating rate fixed at 20 °C min^{-1}, followed by cooling down the post-heated ZnO NW arrays at room temperature. The samples annealed in the air atmosphere at 350, 400, and 450 °C are called as 'ZnO-Air 350', 'ZnO-Air 400', and 'ZnO-Air 450', respectively. It was seen that the annealed ZnO NWs in the air at 400 °C showed better quality. Hence, study the effect of various atmosphere annealing on properties of ZnO NWs was performed at 400 °C. Further, the samples annealed at the certain temperature of 400 °C in pure oxygen and argon atmospheres were named 'ZnO-O_2 400' and 'ZnO-Ar 400', respectively. To avoid confusing the specimens, they are presented in table 1 as some codes.

2.3. Fabrication of UV photodetector

The formation of Ohmic contacts was carried out by thermal evaporating of Ag (150 nm) on ZnO NWs with an interdigitated mask plate. The mask was made of steel, and it is placed on the top of uneven nanowires to

Table 1. Abbreviation form of samples' name.

Samples	Atmosphere	Temperature (°C)
ZnO-Air 350	Air	350
ZnO-Air 400	Air	400
ZnO-Air 450	Air	450
ZnO-O_2 400	O_2	400
ZnO-Ar 400	Ar	400

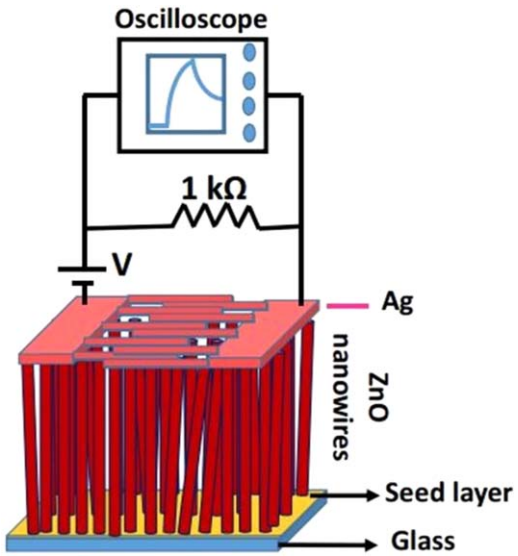

Figure 1. Schematic of the configuration of Ag:ZnO: Ag MSM planar structure in addition to the bias circuit.

fabricate the continuous electrodes. Under Ag coating onto the sample via mask, two interdigitated Ag electrodes are formed on the ZnO NWs. The interdigitated electrodes consisted of five fingers with an inter-spacing of 400 μm. The fingers of the Ag contact electrodes were 0.25 mm wide and 4 mm long. Figure 1 details the schematic cross-section view of our photodetector.

2.4. Characterization

The crystalline structure of the ZnO NWs was investigated by x-ray diffraction (XRD) with a Panalytical X'Pert Pro MPD, Netherland, equipped with a CuKα radiation (wavelength $\lambda = 1.5418$°A). The top and cross-section morphology of the ZnO NW arrays was examined by a field emission scanning electron microscope (FESEM) (Mira 3-XMU, Tescan USA). The optical characterization of the ZnO NWs was determined using the ultraviolet–visible (UV–vis) spectroscopy (Shimadzu Corp., 1800, Japan) and at room temperature photoluminescence spectroscopy (Perkin-Elmer, LS55, USA). Current-voltage (I–V) characteristics were measured by an Agilent 414HB semiconductor parameter analyzer in darkness and under illumination of 373 nm UV light. All measurements were performed in the ambient air at room temperature.

3. Results and discussion

3.1. Structural and morphology characteristics of ZnO nanowire arrays

The XRD spectra of ZnO NWs obtained by chemical bath deposition and annealed at different temperatures in various atmospheres are shown in figures 2(a) and (b). All the annealed ZnO NWs had a hexagonal wurtzite structure. The XRD data revealed that the main peak corresponds to the (002) diffraction plane of the hexagonal ZnO crystal structure. The Scherrer equation was used to calculate the crystallite size (D) of the samples [41]:

$$D = 0.9\lambda/\beta \cos\theta \tag{1}$$

Where λ is the wavelength of incident x-ray from XRD, β is the full width at half maximum (FWHM) measured in radians, and θ is the Bragg angle of diffraction peak. With these values, equation (1) provide the crystallite size and crystallinity percent for the tested samples in table 2. Among the samples annealed in an air atmosphere, ZnO-Air 400 was annealed at a higher intensity and produced a crystallinity increased to 37% and crystallite size

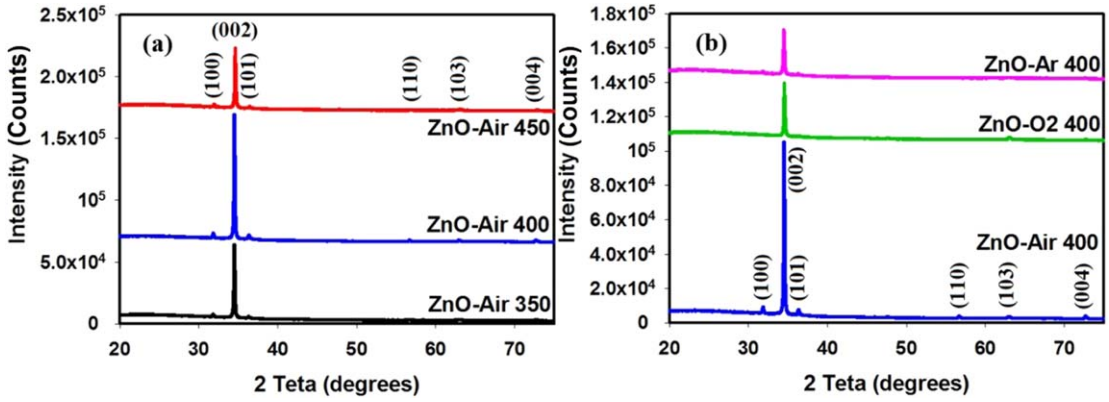

Figure 2. XRD pattern of the ZnO NWs annealing (a) under different temperatures in air, and (b) in various atmospheres.

Table 2. The crystallite size and crystallinity percent as a function of the annealing temperature and environment atmospheres.

Sample	ZnO-Air 350	ZnO-Air 400	ZnO-Air 450	ZnO-O_2 400	ZnO-Ar 400
Crystallite size (nm)	59.28	46.44	60.12	64.64	54.18
Crystallinity (%)	25	37	22.5	18	14

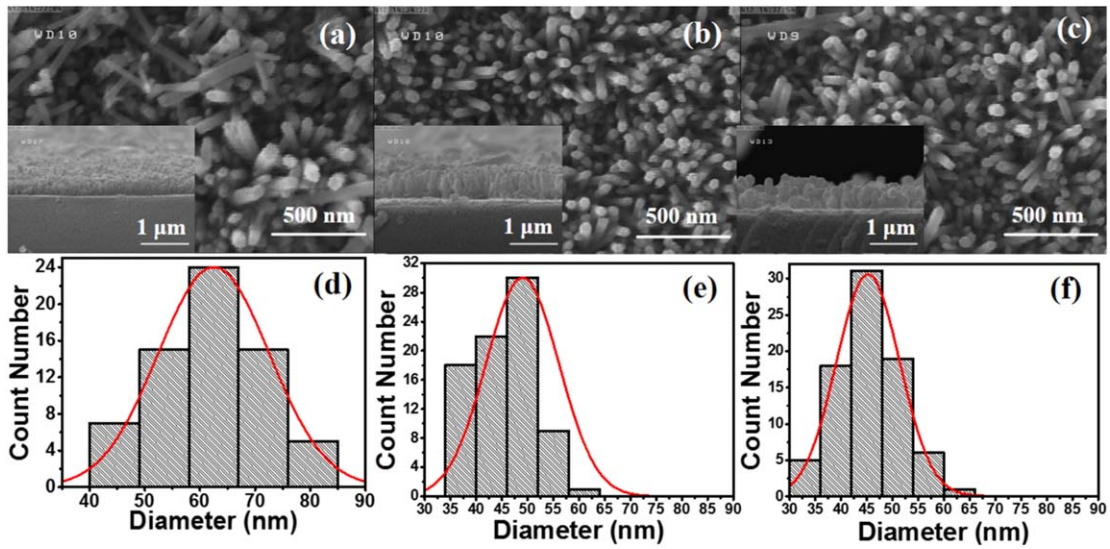

Figure 3. The top views of FESEM images of ZnO NWs grown on glass seeded substrates annealed in an air atmosphere at different temperatures: (a) 350 °C, (b) 400 °C, and (c) 450 °C. Inset of each figure represents cross-section image for the corresponding ZnO NWs. The corresponding diameter histogram ZnO NWs grown on glass seeded substrates annealed in an air atmosphere at (d) 350 °C, (e) 400 °C, and (f) 450 °C.

decreased to 46 nm. These results indicate that crystallinity of ZnO NWs is improved at 400 °C. With varying the atmosphere of post-annealing, the intensity of ZnO-O_2 400 and ZnO-Ar 400 decreased in compared with that of ZnO-Air 400; probably because of the increased defects during the post-annealing in oxygen and argon atmospheres that will be discussed later.

Figures 3(a)–(c) shows the FESEM surface morphology images of the ZnO NW arrays annealed at 350, 400, and 450 °C in the air. The insets in figure 3 show the cross-section images of the samples. Figures 3(d)–(f) represents the distribution of diameters was obtained by averaging 100 nanowires in top-view FESEM images. We see shows that the ZnO NWs grow vertically and closely packed on the ZnO seed layers, the gap between ZnO NWs is negligible, and the thickness of ZnO NWs annealed at different temperatures in the air is 300–600 nm. According to the diameter histogram, as shown in figures 3(d)–(f), the average diameters of the NWs of ZnO-Air 350, ZnO-Air 400, and ZnO-Air 450 is around 62 nm, 49 nm, and 45 nm, respectively. The red solid line in the histograms of ZnO NWs diameters is the corresponding Gaussian line-fitting. In the air

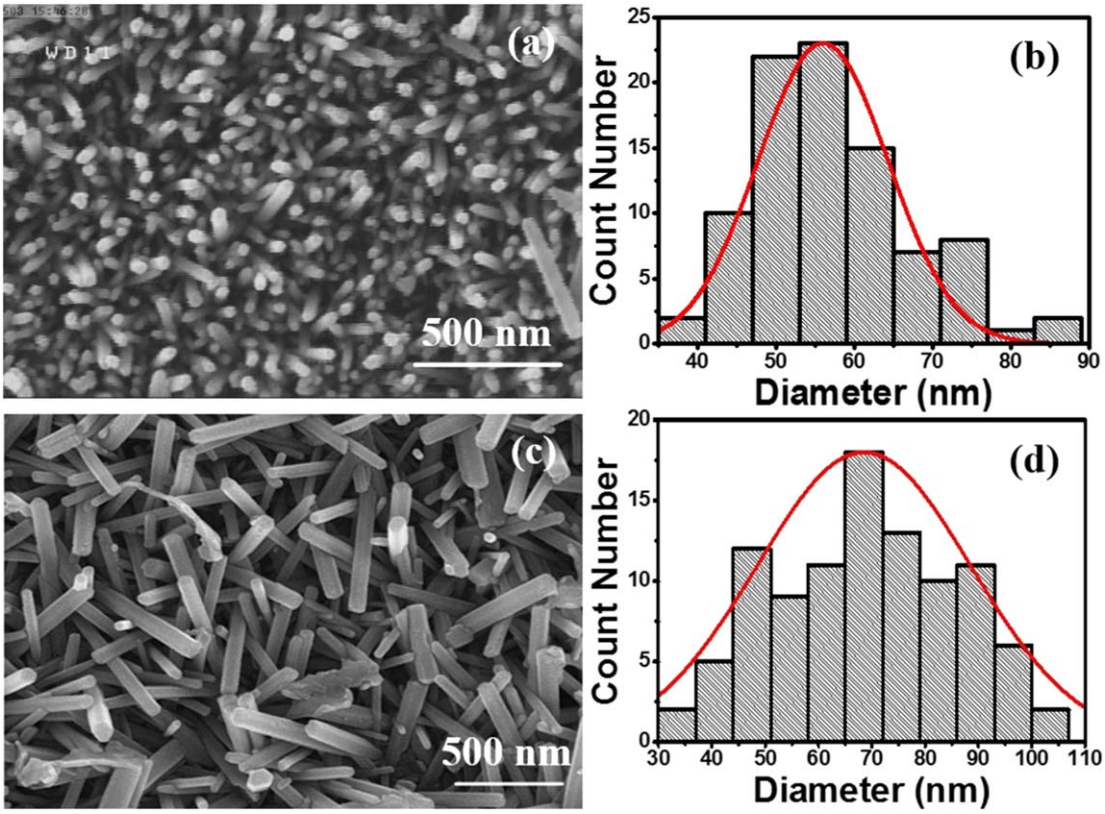

Figure 4. (a) The FESEM micrographs and (b) diameter distribution histograms of ZnO NWs annealed at 400 °C in pure O_2 atmosphere; (c) The FESEM micrographs and (d) diameter distribution histograms of ZnO NWs annealed at 400 °C in pure Ar atmosphere.

atmosphere, the average diameter decreases with increasing the annealing temperature. As seen in FESEM images (figure 3), at 350 °C there is a slight collapse between nanowires, but at 400 °C, the growth rate of the nanowires is improved, and at 450 °C, a little bit of vertical growth decreases.

Figure 4 presents the FESEM micrographs of the ZnO NWs in pure oxygen and argon atmosphere. The diameter distributions of the ZnO NWs annealed at 400 °C in pure oxygen and argon atmospheres, taken from the corresponding FESEM images, are shown in figures 4(b) and (d). The dimensions of the ZnO NWs were measured as 56 and 68.5 nm for ZnO-O_2 400 and ZnO-Ar 400, respectively. A clear difference in the surface morphology of samples annealed in the various atmosphere is presented in the images. The figure shows an almost vertical growth of the NWs for ZnO-Air 400 (figure 3(b)) and especially ZnO-O_2 400 (figure 4(a)) and arbitrarily distributed NWs for ZnO-Ar 400 (figure 4(c)). The FESEM images indicate that some modifications occurred on the surface when the sample was annealed in the pure oxygen atmosphere. Increasing the average diameter of the nanowires, with their vertical growth, magnifies the effective surface area and raises the performance of the photodetector.

3.2. Optical properties

Figures 5(a), (b) represent the typical UV–vis spectra of the ZnO NWs annealed at different temperatures and various atmospheres. A single absorption peak for each annealed sample further reveals their good optical properties [42]. As illustrated in figure 5, the ZnO NWs have a low absorbance in the visible region in addition to high absorbance in the ultraviolet region. It is also observed that ZnO-Air 350 exhibits an absorption edge at about 395 nm. The absorption edge for all samples is located in the range of 380–395 nm.

Figure 6 shows room temperature photoluminescence (PL) spectra (excited at 320 nm, 20 nm slit width) of the ZnO NW arrays grown on the seeded glass layers at different temperatures of 350, 400, and 450 °C for 1 h, respectively. It can be seen from these spectra that the Gaussian curves fitted the PL curves perfectly. The sum of all Gauss-fitted curves is shown by dotted curves. The PL spectra of ZnO NWs annealed at 350 °C in an air atmosphere show the resolved emission peaks at 376 and 597 nm (figure 6(b)). Two peaks at 375 and 591 nm are shown for ZnO NWs annealed at 400 °C (figure 6(c)). Two main peaks at 374 and 589 nm are also absorbed by sample annealed at 450 °C in the air from figure 6(d). Peak 1 for all samples, which is around 375 nm, is related

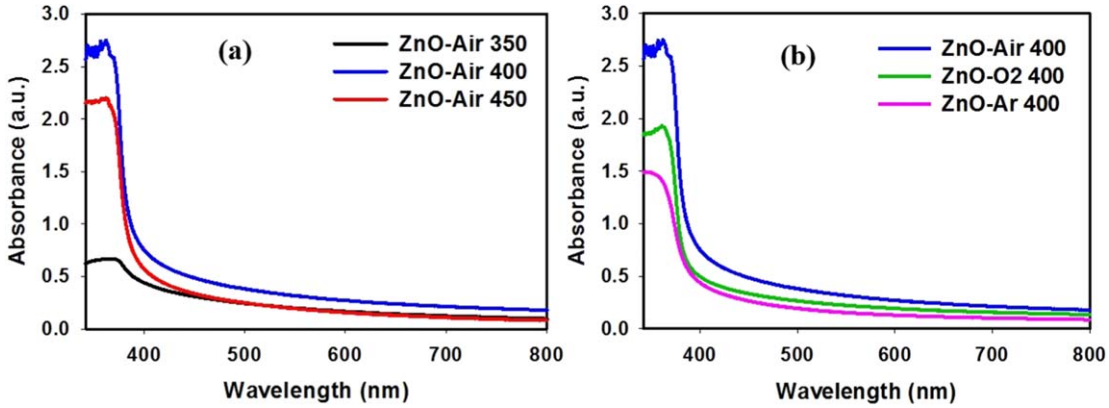

Figure 5. UV–vis absorbance spectra of ZnO NWs annealed at: (a) different temperatures in an air atmosphere, (b) 400 °C in various atmospheres.

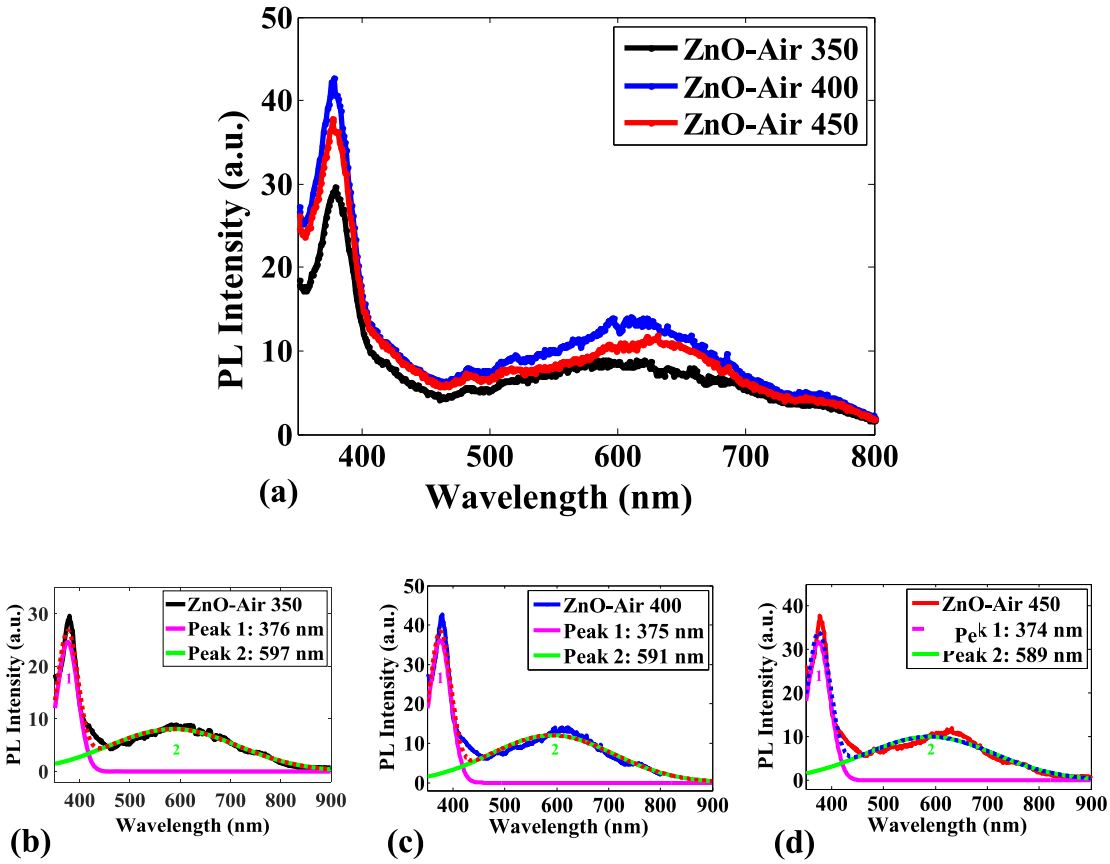

Figure 6. The PL spectra of ZnO NWs (a) annealed at different temperatures in the air; and the two reproducing the PL spectrums for each annealing temperature by two Gaussian components presented in (b)–(d).

to the near-band-edge emission that originates from an exciton transition [35, 43–45]. While peak 2 corresponds to the orange light emission, which is assigned to interstitial oxygen (O_i) [46].

Figures 7(a)–(c) shows the room temperature PL spectra of the ZnO NWs annealed at 400 °C in three different atmospheres. For the PL spectra of ZnO-O_2 400 (figure 7(b)), a UV peak was observed at ~396 nm that is indexed to the recombination of free exciton; i.e., the band edge emission of ZnO NWs [44, 47]. Another peak was observed at 424 nm that is indexed to violet emission [48, 49]. Finally, the third peak was observed at 482 nm. The PL spectra of ZnO-Ar 400 have two peaks at ~407 and 460 nm. The peak at 407 nm corresponding to violet emission. Further, Fan *et al* [48] reported the single violet emission from ZnO without any accompanying deep level emission and UV-emission. The emission centered at 460 nm is attributed to defect states originate from Interstitial Zn (Zn_i) in ZnO [50]. As previously shown in figure 6, the samples annealed at

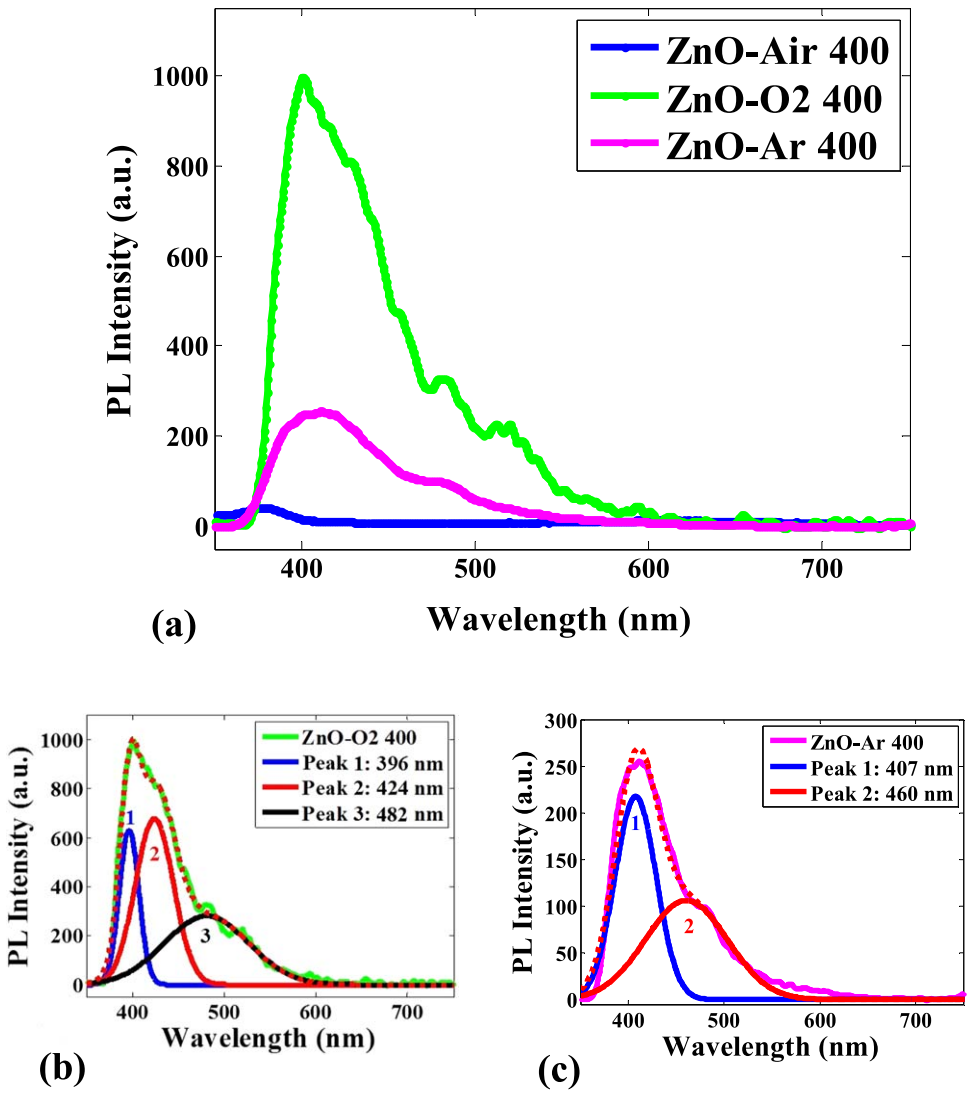

Figure 7. Room temperature PL spectra of: (a) the ZnO-Air 400, ZnO-O_2 400 and ZnO-Ar 400 samples; and Deconvoluted individual peaks by Gaussian line shape function shown in (b) and (c).

Table 3. Comparison of the Gauss-Fitted PL Peak Positions of the ZnO NWs annealed at different temperatures and various ambient atmospheres.

Sample	ZnO-Air 350	ZnO-Air 400	ZnO-Air 450	ZnO-O_2 400	ZnO-Ar 400
Peak Position 1, nm	376	375	374	396	407
Peak Position 2, nm	597	591	589	424	460
Peak Position 3, nm	—	—	—	482	—

400 °C in the air have two main peaks in UV and orange-red spectral range. The orange-red emission is believed to be due to band transition from Zn_i to O_i defect levels in ZnO [51].

As the ZnO NWs were annealed in O_2, the structural defects are increased; and no peak indexing to UV region is observed for the sample annealed in Ar atmosphere. However, ZnO-O_2 400 has a remarkably sharp and intense UV peak. The figure also shows that post-annealing in oxygen reduces the dangling bonds, leading to the increased intensity of UV emission [52]. Argon is an inert gas that does not participate in reactions, but post-annealing in argon enhances the relaxation of prepared samples. Detail of the Gauss-Fitted PL Peak Positions of the ZnO NWs annealed at different temperatures, and various ambient atmospheres is mentioned in table 3. Based on the above discussion, a model for the observed PL emission is demonstrated on an energy band diagram in figure 8.

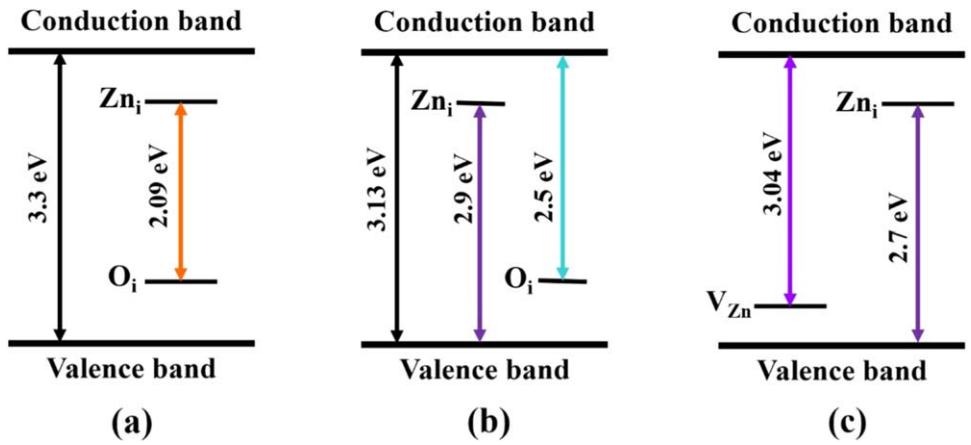

Figure 8. Schematic diagram of the photoluminescence mechanism in ZnO NWs were annealed at 400 °C in (a) air, (b) oxygen and (c) argon for 1 h.

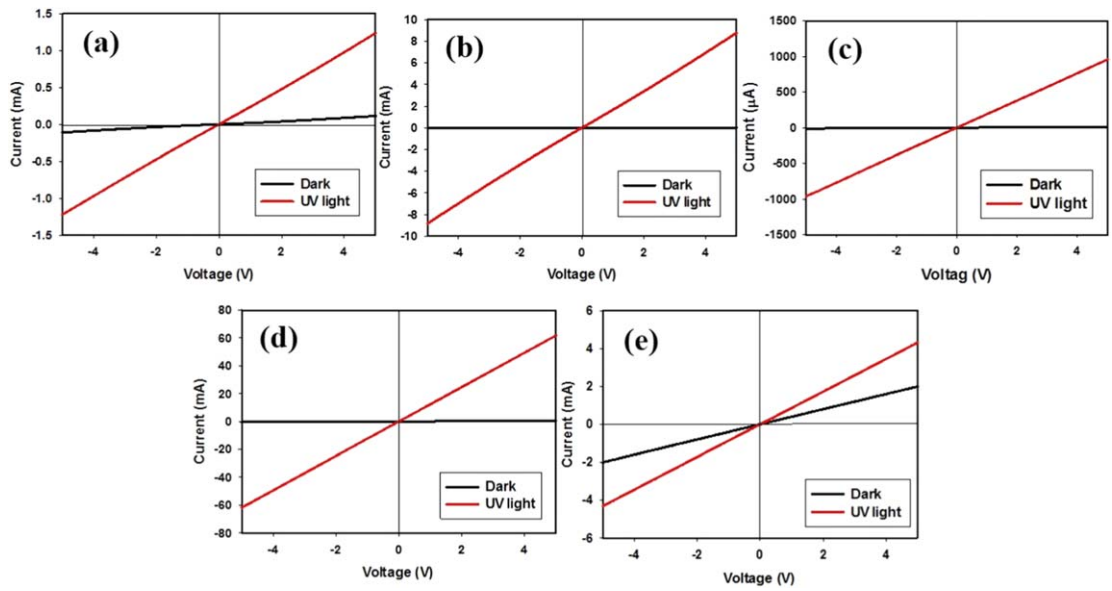

Figure 9. Current versus voltage diagrams for a ZnO NW film device in the dark and under illumination at 373 nm; samples were annealed at (a) 350 °C, (b) 400 °C, and (c) 450 °C in air and annealed at 400 °C in (d) pure oxygen and (e) pure argon atmospheres.

3.3. Electrical characteristics and photoresponse of synthesized ZnO NWs

Figures 9(a)–(e) compares the I–V curves measured in the dark and under UV-light exposure at room temperature in the ambient atmosphere. For photocurrent measurements, the peak wavelength of the excitation light source was 373 nm, and the incident optical power was 85.3 μW. As shown in figures 9(a)–(e), there is a significant difference in conductivity between the sample under dark conditions and the one under UV illumination. The linearity of I–V response suggests the ohmic contact between the ZnO film and Ag electrodes [53]. The responsivity (R) of the detector, defined as a ratio of the steady-state photocurrent $I_{ph} = I_{light} - I_{dark}$ to the incident optical power P_{opt} [54], is also obtained from figures 9(a)–(e):

$$R = I_{ph}/P_{opt} \tag{2}$$

From the results of figure 9, the responsivity is obtained as 3.14, 7.33, and 3.66 A W^{-1} for the photodetectors of ZnO NWs annealed at 350, 400, and 450 °C in the air, respectively. The responsivity values of ZnO-O_2 400 and ZnO-Ar 400 were measured as 10.31 and 3.14 A W^{-1}, respectively. It should be mentioned that the responsivity results presented here are higher than those reported by Mohite *et al* [55]. Also, the best responsivity is obtained for the sample annealed in pure oxygen.

To confirm the sensitivity of UV photodetectors, the responsivity of the samples under UV illumination with a wavelength of 373 nm is shown in table 4.

Table 4. The responsivity of the ZnO NWs annealed at different temperatures and various ambient atmospheres under UV light illumination.

Sample	ZnO-Air 350	ZnO-Air 400	ZnO-Air 450	ZnO-O_2 350	ZnO-O_2 400	ZnO-O_2 450	ZnO-Ar 350	ZnO-Ar 400	ZnO-Ar 450
Responsivity (A/W)	3.14	7.33	3.66	11.01	10.31	24.49	0.79	3.14	1.25

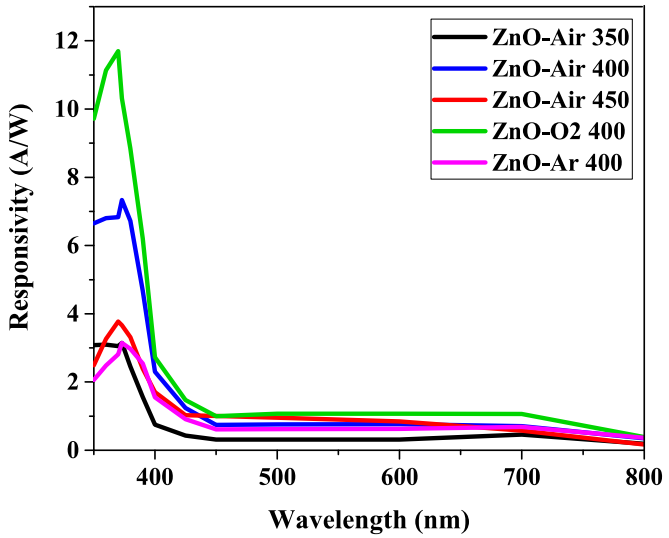

Figure 10. Spectral responsivity of the ZnO UV photodetectors at 5 V applied bias.

The reported values for responsivity indicate the proper quality of ZnO NWs under annealing for use in UV photodetectors. The values listed in table 4 show better results than those given in [56, 57].

The corresponding external quantum efficiency of the detector is defined as [58]:

$$\eta = \frac{hc}{q\lambda}R = 1240\frac{R}{\lambda} \tag{3}$$

where, h is the Planck's constant, c is the light velocity, and λ is the light wavelength. The quantum efficiency increased from about 5% to 14.82% and 13.28%, respectively as the samples were annealed in pure oxygen and Ar. The results indicate that annealing in oxygen has a significant effect on the electrical properties.

ZnO is the n-type semiconductor due to lack of oxygen and Zn ion vacancies. Oxygen molecules in the air ambient in which are absorbed on the surface of nanowires and a depletion layer with low conductivity near the surface of the nanowires is formed ($O_2(gas) + e^- \rightarrow O_2^-(adsorbed)$).

Under the UV illumination, a pair of electron-hole is photogenerated, the holes migrate to the surface of the nanowires, which have negative-oxygen ions. As a result, electrons find the chance to participate in the conduction band without risk of recombination and increase photocurrent [59, 60].

In the sample post-annealed in an oxygen atmosphere at 400 °C, peaks corresponding to defects of Zn_i and O_i are observed in PL spectra (figure 7). Since the peak intensity of Zn_i is higher than that of O_i and is also higher than the sample of ZnO-Ar 400, it is expected that increasing Zn_i defects in ZnO will be responsible for increasing the flow of light.

Figure 10 shows the responsivity of the fabricated ZnO thin film photodetector devices. Maximum response is found in the wavelength range 360 nm to 380 nm. The maximum responsivity of the ZnO UV photodetectors under illumination of 370 nm is obtained. The photocurrent drops drastically, which reveals high UV light sensitivity of ZnO for solar blind UV detector.

The photoconductivity can be recorded as soon as the film conductivity is stabilized with an applied electric field. The photoconductivity transients were performed with the illuminated light of 373 nm under an applied 5 V bias. Figures 11(a)–(e) shows the results of transient photocurrent measurements for the ZnO NWs. The photoconductivity transient curve is fitted well with an exponential curve as follows [61, 62]:

$$\alpha_{ph} = \alpha_s(1 - e^{-t/\tau}) \tag{4}$$

Where α_{ph} is the transient photoconductivity, α_s is the steady photoconductivity value, t is the time, and τ is the relaxation time constant. The rise time is defined as the current increases up to 63% of the peak. Table 5

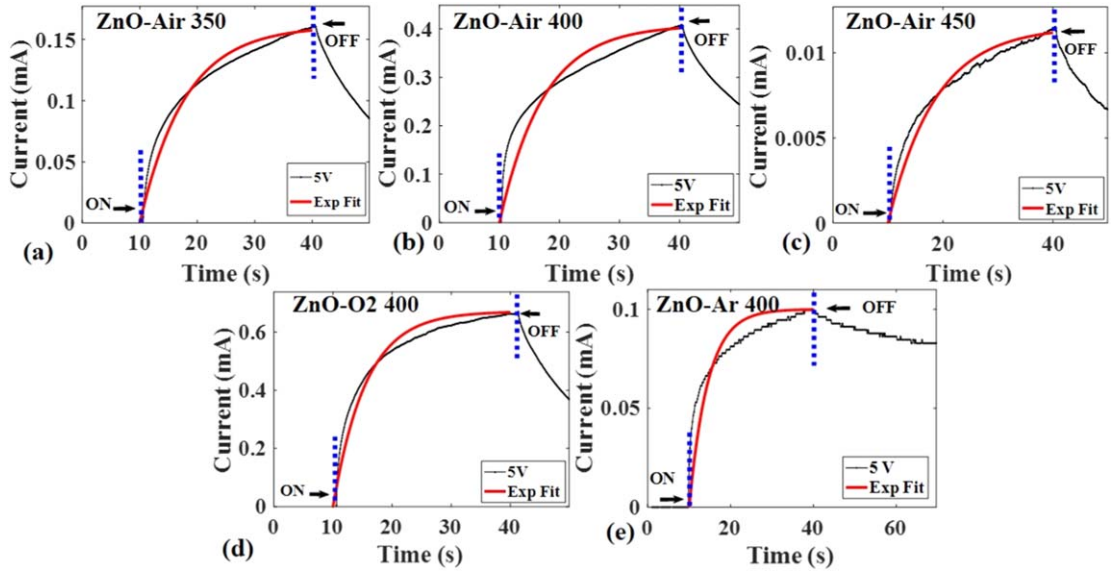

Figure 11. Photoconductivity transients of ZnO NWs (a)–(c) at different annealing temperatures in air ambient; the graphs (d) and (e) shows the results of the ZnO NWs annealed at the various environment. In each graph, the best exponential fit for the transient current is also shown.

Table 5. The rise time of photodetectors based on ZnO NWs post-annealed at different temperatures and atmospheres according to different bias voltages.

	Bias voltage (V)				
Sample	1	3	5	7	10
ZnO-Air 350	9.21	9.20	7.82	7.05	5.51
ZnO-Air 400	11.10	8.45	7.27	5.94	6.55
ZnO-Air 450	10.12	8.53	8.57	6.77	7.28
ZnO-O_2 350	9.20	5.21	5.32	3.59	2.81
ZnO-O_2 400	6.17	6.70	5.54	6.39	8.41
ZnO-O_2 450	7.08	4.16	3.16	2.98	1.34

summarizes the response time of UV photodetectors based on post-annealed ZnO NWs in different temperatures in the air and the oxygen, and the corresponding τ values obtained from the fitted curve is also included. It is noted from the table 5 that the response speed of samples prepared in the oxygen atmosphere is higher than those of the samples prepared in the air.

4. Conclusion

In the present study, we successfully grew the ZnO nanowire (NW) arrays by the low-price commercial CBD method at a low temperature. The XRD results approve that the high-quality crystallinity ZnO NWs had a wurtzite hexagonal structure and grew in (002) direction, which are consistent with FESEM micrographs. A strong UV emission was detected in all PL spectra. Among the samples annealed in various temperatures in air, the ZnO NWs annealed at 400 °C indicated a better quality for UV detection. Also, we found that annealing the sample in pure oxygen atmosphere considerably improves the UV detection characteristics of the ZnO NWs.

ORCID iDs

R Bahramian https://orcid.org/0000-0002-2291-4108
A Moshaii https://orcid.org/0000-0002-5708-3949

References

[1] Kung C Y *et al* 2013 Influence of Li doping on the optical and magnetic properties of ZnO nanorods synthesized by low temperature hydrothermal method *Thin Solid Films* **529** 181–4

[2] Schmidt-Mende L and MacManus-Driscoll J L 2007 ZnO–nanostructures, defects, and devices *Mater. Today* **10** 40–8

[3] Yang C, Li Q, Tang L, Bai A, Song H and Yu Y 2016 Monodispersed colloidal zinc oxide nanospheres with various size scales: synthesis, formation mechanism, and enhanced photocatalytic activity *J. Mater. Sci.* **51** 5445–59

[4] Jandow N N, Abu Hassan H, Yam F K and Ibrahim K 2012 Comparative study of the properties of ZnO thin films deposited on poly propylene carbonate (PPC) and glass substrates *J. Mater. Sci.* **47** 1972–6

[5] Cerrato E, Gionco C, Berruti I, Sordello F, Calza P and Paganini M C 2018 Rare earth ions doped ZnO: Synthesis, characterization and preliminary photoactivity assessment *J. Solid State Chem.* **264** 42–7

[6] Oliveira F F, Proenca M P, Araújo J P and Ventura J 2016 Electrodeposition of ZnO thin films on conducting flexible substrates *J. Mater. Sci.* **51** 5589–97

[7] Lee W, Dwivedi R P, Hong C, Kim H W, Cho N and Lee C 2008 Enhancement of the electrical properties of Al-doped ZnO films deposited on ZnO-buffered glass substrates by using an ultrathin aluminum under layer *J. Mater. Sci.* **43** 1159–61

[8] Chen Y, Zeng X, Zhou Y, Li R, Yao H, Cao X and Jin P 2018 Core–shell structured Cs_xWO_3@ZnO with excellent stability and high performance on near-infrared shielding *Ceram. Int.* **44** 2738–44

[9] Marimuthu T, Anandhan N and Thangamuthu R 2018 Electrochemical synthesis of one-dimensional ZnO nanostructures on ZnO seed layer for DSSC applications *Appl. Surf. Sci.* **428** 385–94

[10] Yang P, Yan H, Mao S, Russo R, Johnson J, Saykally R, Morris N, Pham J, He R and Choi H J 2002 Controlled growth of ZnO nanowires and their optical properties *Adv. Funct. Mater.* **12** 323

[11] Cheng J, Zhang Y and Guo R 2008 ZnO microtube ultraviolet detectors *J. Cryst. Growth* **310** 57–61

[12] Sun Y, Zhang X, Tian C, Jiang D, Li Z and Liu S 2015 Varying load resistances of zinc oxide ultraviolet photodetectors: a simple method to change responsivity *Mater. Sci. Semicond. Process.* **31** 10–3

[13] Farhat O F, Halim M M, Ahmed N M and Qaeed M A 2016 ZnO (NFs) growth from ZnO (NRs) by Controlling Growth Temperature on flexible Teflon substrate by CBD technique for UV photodetector *Superlattices Microstruct.* **100** 1120–7

[14] Chung R J, Wang H Y, Li Y C and Yeh P H 2013 Preparation and sensor application of carbon coated zinc oxide nanorods array *J. Aust. Ceram. Soc.* **49** 81–8

[15] Meng Y, Lin Y, Lin Y and Yang J 2014 Preparation and surface modification of hierarchical nanosheets-based ZnO microstructures for dye-sensitized solar cells *J. Solid State Chem.* **210** 160–5

[16] Shaban Z, Majles Ara M H, Falahatdoost S and Ghazyani N 2016 Optimization of ZnO thin film through spray pyrolysis technique and its application as a blocking layer to improving dye sensitized solar cell efficiency *Curr. Appl. Phys.* **16.2** 131–4

[17] Wang G, Li Z, Li M, Feng Y, Li W and Liao S L , J 2018 Synthesizing Vertical Porous ZnO Nanowires Arrays on Si/ITO Substrate for Enhanced Photocatalysis *Ceram. Int.* **44** 1291–5

[18] Yu Z, Moussa H, Liu M, Schneider R, Moliere M and Liao H 2018 Solution precursor plasma spray process as an alternative rapid one-step route for the development of hierarchical ZnO films for improved photocatalytic degradation *Ceram. Int.* **44** 2085–92

[19] Ahmed A A, Devarajan M and Afzal N 2017 Fabrication and characterization of high performance MSM UV photodetector based on NiO film *Sensors and Actuators A: Physical* **262** 78–86

[20] Rogers D J, Teherani F H, Yasan A, Minder K, Kung P and Razeghi M 2006 Electroluminescence at 375 nm from a ZnO/GaN: Mg/c-Al_2O_3 heterojunction light emitting diode *Appl. Phys. Lett.* **88** 141918

[21] Xu W Z, Ye Z, Zeng Y, Zhu L, Zhao B, Jiang L, Lu J and Zhang S 2006 ZnO light-emitting diode grown by plasma-assisted metal organic chemical vapor deposition *Appl. Phys. Lett.* **88** 1–3

[22] Meléndrez M F, Hanks K, Leonard-Deepak F, Solis-Pomar F, Martinez-Guerra E, Pérez-Tijerina E and José-Yacaman M 2012 Growth of aligned ZnO nanorods on transparent electrodes by hybrid methods *J. Mater. Sci.* **47** 2025–32

[23] Sahu V K, Misra P, Ajimsha R S, Das A K and Singh B 2016 Effect of growth temperature on diode parameters of n-ZnO/p-Si heterojunction diodes grown by atomic layer deposition *Mater. Sci. Semicond. Process.* **54** 1–5

[24] Farhat O F, Halim M M, Ahmed N M, Oglat A A, Abuelsamen A A, Bououdina M and Qaeed M A 2017 A study of the effects of aligned vertically growth time on ZnO nanorods deposited for the first time on Teflon substrate *Appl. Surf. Sci.* **426** 906–12

[25] Molefe F V, Koao L F, Dejene B F and Swart H C 2015 Phase formation of hexagonal wurtzite ZnO through decomposition of Zn (OH)2 at various growth temperatures using CBD method *Opt. Mater.* **46** 292–8

[26] Kumar Y, Rana A K, Bhojane P, Pusty M, Bagwe V, Sen S and Shirage P M 2015 Controlling of ZnO nanostructures by solute concentration and its effect on growth, structural and optical properties *Mater. Res. Express* **2** 105017

[27] Kim J, Hyeon Baik K and Jang S 2016 Schottky contact on hydrothermally grown a-plane ZnO for hydrogen sensing and UV detection *Curr. Appl. Phys.* **16** 221–5

[28] Tan W K, Razak K A, Lockman Z, Kawamura G, Muto H and Matsuda A 2014 Synthesis of ZnO nanorod–nanosheet composite via facile hydrothermal method and their photocatalytic activities under visible-light irradiation *J. Solid State Chem.* **211** 146–53

[29] Klubnuan S, Suwanboon S and Amornpitoksuk P 2016 Effects of optical band gap energy, band tail energy and particle shape on photocatalytic activities of different ZnO nanostructures prepared by a hydrothermal method *Opt. Mater.* **53** 134–41

[30] Zhu L, Li Y and Zeng W 2018 Hydrothermal synthesis of hierarchical flower-like ZnO nanostructure and its enhanced ethanol gas-sensing properties *Appl. Surf. Sci.* **427** 281–7

[31] Wu J J, Wen H I, Tseng C H and Liu S C 2004 Well-aligned ZnO Nanorods via hydrogen treatment of ZnO films *Adv. Funct. Mater.* **14** 806–10

[32] Shabannia R and Hassan H A 2013 Growth and characterization of aligned ZnO nanorods synthesized on porous silicon *Mater. Lett.* **98** 135–7

[33] Polat I, Yılmaz S, Bacaksız E, Atasoy Y and Tomakin M 2014 Synthesis and fabrication of Mg-doped ZnO-based dye-synthesized solar cells *J Mater Sci: Mater Electron* **25** 3173–8

[34] Giri P K, Dhara S and Chakraborty R 2010 Effect of ZnO seed layer on the catalytic growth of vertically aligned ZnO nanorod arrays *Mater. Chem. Phys.* **122** 18–22

[35] Bahramian R, Moshaii A and Eshghi H 2016 Effect of seeding modification of substrate on the growth and UV detection properties of ZnO nanowires *Mater. Lett.* **179** 222–5

[36] Ng Z N, Chan K Y and Tohsophon T 2012 Effects of annealing temperature on ZnO and AZO films prepared by sol–gel technique *Appl. Surf. Sci.* **258** 9604–9

[37] Purohit A, Chander S, Sharma A, Nehra S P and Dhaka M S 2015 Impact of low temperature annealing on structural, optical, electrical and morphological properties of ZnO thin films grown by RF sputtering for photovoltaic applications *Opt. Mater.* **49** 51–8
[38] Uthirakumar P and Hong C-H 2009 Effect of annealing temperature and pH on morphology and optical property of highly dispersible ZnO nanoparticles *Mater. Charact.* **60.11** 1305–10
[39] Bahramian R, Eshghi H and Moshaii A 2016 Influence of annealing temperature on morphological, optical and UV detection properties of ZnO nanowires grown by chemical bath deposition *Mater. Des.* **107** 269–76
[40] Abuelsamen A A, Mahmud S, Seeni A, Kaus N H M and Farhat O F 2017 Effects of precursor concentrations on the optical and morphological properties of ZnO nanorods on glass substrate for UV photodetector *Superlattices Microstruct.* **111** 536–45
[41] Kuo S Y, Chen W C and Cheng C P 2006 Investigation of annealing-treatment on the optical and electrical properties of sol–gel-derived zinc oxide thin films *Superlattices Microstruct.* **39** 162–70
[42] Umar A, Kumar R, Kumar G, Algarni H and Kim S H 2015 Effect of annealing temperature on the properties and photocatalytic efficiencies of ZnO nanoparticles *J. Alloys Compd.* **648** 46–52
[43] Mhlongo G H, Motaung D E, Nkosi S S, Swart H C, Malgas G F, Hillie K T and Mwakikunga B W 2014 Temperature-dependence on the structural, optical, and paramagnetic properties of ZnO nanostructures *Appl. Surf. Sci.* **293** 62–70
[44] Rajan A, Yadav H K, Gupta V and Tomar M 2013 Sol–gel derived Ag-doped ZnO thin film for UV photodetector with enhanced response *J. Mater. Sci.* **48** 7994–8002
[45] Kunj S and Sreeniva K 2016 Residual stress and defect content in magnetron sputtered ZnO films grown on unheated glass substrates *Curr. Appl. Phys.* **16** 748–56
[46] Djurišić A B, Leung Y H, Tam K H, Ding L, Ge W K, Chen H Y and Gwo S 2006 Green, yellow, and orange defect emission from ZnO nanostructures: influence of excitation wavelength *Appl. Phys. Lett.* **88.10** 103107
[47] Willander M, Nur O, Bano N and Sultana K 2009 Zinc oxide nanorod-based heterostructures on solid and soft substrates for white-light-emitting diode applications *New J. Phys.* **11** 125020
[48] Fan X M, Lian J S, Zhao L and Liu Y H 2005 Single violet luminescence emitted from ZnO films obtained by oxidation of Zn film on quartz glass *Appl. Surf. Sci.* **252** 420–4
[49] Sreedhar A, Kwon J H, Yi J, Kim J S and Gwag J S 2016 Enhanced photoluminescence properties of Cu-doped ZnO thin films deposited by simultaneous RF and DC magnetron sputtering *Mater. Sci. Semicond. Process.* **49** 8–14
[50] Bandopadhyay K and Mitra J 2015 Zn interstitials and O vacancies responsible for n-type ZnO: what do the emission spectra reveal? *RSC Adv.* **5** 23540
[51] Alvi N H, Ul Hasan K, Nur O and Willander M 2011 The origin of the red emission in n-ZnO nanotubes/p-GaN white light emitting diodes *Nanoscale Res. Lett.* **6** 1–7
[52] Panda D and Tseng T Y 2013 One-dimensional ZnO nanostructures: fabrication, optoelectronic properties, and device applications *J. Mater. Sci.* **48** 6849–77
[53] Moore J C and Thompson C V 2013 A phenomenological model for the photocurrent transient relaxation observed in ZnO-based photodetector devices *Sensors* **13** 9921–40
[54] Zhang H, Babichev A V, Jacopin G, Lavenus P, Julien F H, Egorov A Y, Zhang J, Pauporté T and Tchernycheva M 2013 Characterization and modeling of a ZnO nanowire ultraviolet photodetector with graphene transparent contact *J. Appl. Phys.* **114** 234505
[55] Mohite S V and Rajpure K Y 2014 Synthesis and characterization of Sb doped ZnO thin films for photodetector application *Opt. Mater.* **36** 833–8
[56] Yua J and Tian N 2016 High spectrum selectivity and enhanced responsivity of ZnO ultraviolet photodetector realized by the addition of ZnO nanoparticles layer *Phys. Chem. Chem. Phys.* **18** 1–7
[57] Ali G M, Moore J C, Kadhim A K and Thompson C 2014 Electrical and optical effects of Pd microplates embedded in ZnO thin film based MSM UV photodetectors: a comparative study *S. A. A.* **209** 16–23
[58] Hazra P, Singh S K and Jit S 2014 Ultraviolet photodetection properties of ZnO/Si heterojunction diodes fabricated by ALD technique without using a buffer layer *J Semicond Tech Sci* **14** 117–23
[59] Soci C, Zhang A, Xiang B, Dayeh S A, Aplin D P R, Park J, Bao X Y, Lo Y H and Wang D 2007 ZnO nanowire UV photodetectors with high internal gain *Nano Lett.* **7** 1003–9
[60] Lupan O, Cretu V, Postica V, Ahmadi M, Cuenya B R, Chow L, Tiginyanu I, Viana B, Pauporté T and Adelung R 2016 Silver-doped zinc oxide single nanowire multifunctional nanosensor with a significant enhancement in response *Sensors Actuators* B **223** 893–903
[61] Zheng X G, Li Q S, Hu W, Chen D, Zhang N, Shi M J, Wang J J and Zhang L C 2007 Photoconductive properties of ZnO thin films grown by pulsed laser deposition *J. Lumin.* **122** 198–201
[62] Zheng X G, Li Q S, Zhao J P, Chen D, Zhao B, Yang Y J and Zhang L C 2006 Photoconductive ultraviolet detectors based on ZnO films *Appl. Surf. Sci.* **253** 2264–7